Energy Structure in Photoelectric Emission from Cs-Covered Silicon and Germanium

F. G. ALLEN* AND G. W. GOBELI
Bell Telephone Laboratories, Murray Hill, New Jersey
(Received 30 November 1965)

Photoelectric yield and energy distributions are given for clean-cleaved and cesium-covered (111) surfaces of silicon and germanium. A monolayer of cesium lowers the work function of each to ~1.6 eV and reveals detailed structure in both yield and distributions. This structure is directly related to that seen in reflectivity and the major features in silicon agree well with those predicted by theoretical calculations of Brust, Cohen, and Phillips, assuming direct transitions in an energy-band model derived by the pseudopotential method. Varying bulk doping from extreme n to p type produces large changes in energy distributions and yield caused by the changes in band bending induced just beneath the surface. Such band-bending effects are much stronger for silicon than for germanium. It is concluded that excitation is predominantly a direct volume process and that emitted electrons originate from a mean depth ranging from 20 Å to several hundred Å as the electron energy varies from 6 to 3 eV above the valence-band maximum.

I. INTRODUCTION

RECENT work on the photoelectric emission from clean silicon and germanium surfaces cleaved in high vacuum[1–6] has yielded information on the effect of band bending on photoemission, surface-state structure, escape length of excited electrons, and excitation processes. The interpretation of the principal emission mechanism for these surfaces as being a direct volume excitation,[2,7,8] together with the published energy-band structure for silicon[9,10] and germanium,[11,12] leads to the expectation that new structure should appear in both yield and energy distributions as a larger range of energies above threshold is examined. One means of increasing this range is to lower the surface barrier with a monolayer of cesium.

Two groups have already reported photoemission results on cesium covered silicon surfaces. Spicer and Simon[13] worked with surfaces cleaned by heating in vacuum, which produced p layers at the surface, while Scheer and van Laar[1] used surfaces of varying dopings cleaved or broken in vacuum. Results of the two studies, while showing basically the same type of yield curve, are in disagreement in details with each other and with the findings to be presented here on silicon. Both works studied only the full monolayer coverage.

The present experiment (a) used only surfaces cleaved *in vacua* of 10^{-10} mm Hg with a high degree of physical perfection, (b) had an independent means of measuring the work function of each surface, (c) used an atomic-beam technique for depositing cesium in very small, measurable doses, (d) measured both yield and energy distributions at all coverages and for a variety of dopings from extreme p to extreme n type. Both cleaved, and cleaved-and-heated surfaces were taken as the starting point. Conclusions of this work indicate that there is considerably more structure in the spectral yield than found previously, and that this structure and that in the energy distributions is explained in most details by direct transitions on the currently accepted energy-band diagram for silicon. Results of work function, yield and energy distribution measurements on cesium-covered germanium surfaces are presented here for the first time.[14]

II. EXPERIMENTAL TECHNIQUES

Cleavage Tube, Components, and Optics

The details of the cleavage technique, which permits the repeated cleavage of surfaces of ~1×0.2 cm cross section *in vacua* of $<2\times10^{-10}$ mm Hg, have been described earlier.[2,3,15] Examination of the cleaved surfaces with the optical microscope, the electron microscope, and by low-energy electron diffraction, indicates that the cleaved surfaces consist of (111) planes several thousand Angstroms in extent and probably atomically flat separated by steps 50–500 Å high. The highly ordered and reproducible atomic structure of the first layer is somewhat different from that of the bulk lattice and undergoes a further modification upon brief annealing in vacuum.[16]

Figure 1 shows the relative placement of components in the bakeable high vacuum tube. The sample A clamped to its supporting platform B can be rotated to face any of the tube elements, and in addition can be

* Present address: Bellcomm Inc., Washington, D. C.
[1] J. van Laar and J. J. Scheer, Philips Res. Repts. **17**, 101 (1962).
[2] G. W. Gobeli and F. G. Allen, Phys. Rev. **127**, 141 (1962).
[3] F. G. Allen and G. W. Gobeli, Phys. Rev. **127**, 150 (1962).
[4] G. W. Gobeli and F. G. Allen, Surface Sci. **2**, 402 (1964).
[5] F. G. Allen and G. W. Gobeli, J. Appl. Phys. **35**, 597 (1964).
[6] G. W. Gobeli and F. G. Allen, Phys. Rev. **137**, A245 (1965).
[7] E. O. Kane, Phys. Rev. **127**, 131 (1962).
[8] G. W. Gobeli, F. G. Allen, and E. O. Kane, Phys. Rev. Letters, **12**, 94 (1964).
[9] D. Brust, M. L. Cohen, and J. C. Phillips, Phys. Rev. Letters, **9**, 389 (1962).
[10] D. Brust, Phys. Rev. **134**, A1337 (1964).
[11] D. Brust, J. C. Phillips, and F. Bassani, Phys. Rev. Letters, **9**, 94 (1962).
[12] M. L. Cohen and J. C. Phillips (private communication). See Fig. 18 of this paper.
[13] W. E. Spicer and R. E. Simon, Phys. Rev. Letters **9**, 395 (1962).
[14] Photoemissive studies on germanium surfaces by Scheer and van Laar are to be reported (private communication).
[15] G. W. Gobeli and F. G. Allen, J. Phys. Chem. Solids **14**, 23 (1960).
[16] J. J. Lander, G. W. Gobeli, and J. Morrison, J. Appl. Phys. **34**, 2298 (1963).

moved with adjusting screws laterally or vertically in three dimensions through a sylphon bellows as required. The cleavage tool H enters from above the sample.

Work function measurements were made by the Kelvin method using a polycrystalline 0.040-in. diam molybdenum reference probe C, vibrated axially close to the sample. The reference surface was then calibrated against a freshly flashed single crystal tungsten ribbon D, whose absolute work function was determined photoelectrically. Null sensitivity was ± 0.005 V and work function determinations are believed accurate to ± 0.05 V. Work function variation over the several square mm of usable surface was within ± 0.010 V for the clean surface. This variation rose to ± 0.15 V during intermediate cesium coverages, and returned to ± 0.03 V for the fully covered surface.

The spectral yield of samples was measured using Hg, Zr, or H_2 arcs as the source for a Bausch and Lomb 500 mm grating monochromator. The light was focused with front-face aluminized mirrors onto the cleaved face of the sample (1 mm$\times$2 mm image) through the quartz window E, and then specularly reflected back out again along the same path. To avoid spurious emission due to the small component of light scattered from the sample surface the photoemission current measured was that leaving the sample with all other tube elements, including the sample supporting structure (insulated from the sample) biased to collect electrons. Uniformity of emission over the cleaved surface was good for both the clean and the full Cs-covered surface, but was poorer at intermediate Cs coverges due to the difficulty in keeping the partial Cs coverage uniform.

Calibration of light intensity was carried out using a Cs_3Sb phototube originally calibrated by Apker and Taft. The sources were sufficiently stable that an accuracy of 5% could be achieved if a calibration run over the complete wavelength range was taken following every one or two sample runs. Data points were taken at emission lines of the sources where available or at short intervals in the continua.

The yield results were divided by $1-R(\lambda)$, where $R(\lambda)$ is the published reflectivity of the surface, to give emitted electrons per *absorbed* photon. In several cases where interesting structure was seen, it was ascertained that this correction only enhanced or reduced somewhat the structure already present in the data, but did not introduce structure where none was present before.

Surface resistivity changes in very high resistivity silicon samples could be monitored during cesium application by pressing the four-point probe G against the cleaved face, with a probe spacing of approximately 1 mm.

Several additional samples were stored in the side arm I, and could be transferred via the chute J, when this was lifted to engage with the sample support. Thus many samples, with several cleavages per sample, could be run without opening the high vacuum station to air.

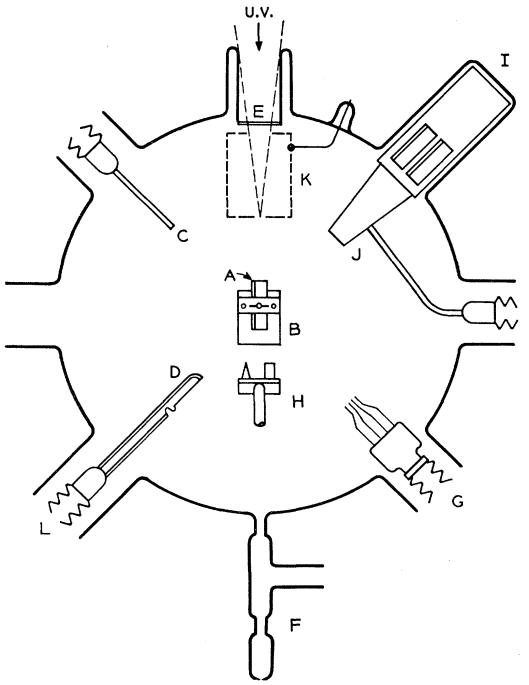

FIG. 1. Diagram of experimental tube. A, sample; B, rotatable supporting platform; C, reference probe; D, tungsten single crystal ribbon; E, quartz window; F, cesium gun; G, four-point probe; H, scribing and cleavage tool; I, sample tray; J, transfer chute; K, mesh retarding-potential enclosure.

Energy Distributions

Total energy distributions of the emitted photoelectrons were measured with the cylindrical mesh enclosure (Fig. 1-K). The cleaved sample surface was inserted into an aperture at one end of this cylinder that fitted closely around the L-shaped sample cross section. With the cleaved face coplanar with the inside of this cage, the fringe fields between the cesium-coated, cleaved face and the uncleaved edges of the sample (a difference of work function of up to 3.3 V) were minimized, though not eliminated. Light entered and returned through a circular aperture at the other end of the enclosure. The 80% transparent mesh minimized undesired photoemission from two sources: (a) that emitted from the enclosure back to the sample during retarding conditions, and (b) that due to light reflected from the enclosure back onto undesired portions of the sample. In addition, the sample was easily visible through the mesh for positioning and focusing the image. The work function of the gold-evaporated molybdenum mesh (never cleaned) remained at 4.55 ± 0.05 eV during the entire set of runs, while the molybdenum boss used for Kelvin measurements (also never cleaned) maintained a work function of 4.50 ± 0.10 eV.

The retarding voltage applied to the cylindrical enclosure was a ramp, linearly rising in time, supplied by an electronic operational amplifier which integrated a battery voltage. This produced an extremely smooth,

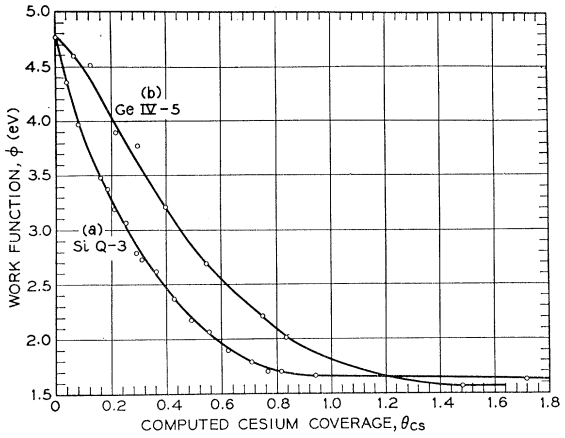

FIG. 2. Work function φ of silicon (a), and germanium (b), versus cesium coverage, θ_{Cs}, in monolayers. $\theta_{Cs}=1$ at 8×10^{14} Cs atoms per cm^2.

constant slope voltage with no short- or long-time cyclic variations. The velocity distributions were displayed directly on an X-Y recorder by using a second operational amplifier to differentiate the sample current as it varied with ramp voltage. Noise was kept below objectionable levels by filtering before and after the differentiator. The ramp slope was kept sufficiently slow to avoid serious distortion due to the filtering.

The geometry described for the energy distributions, forced upon the experiment by the cleavage technique, together with the fringe fields at sample edges after Cs deposition, introduced certain distortions in the energy distributions. These are discussed in the Appendix, where it is shown that they occur principally at low kinetic energies and do not detract seriously from the information available.

Cesium Application and Its Effect

Cesium ions were applied to the sample surface in small controlled doses by the atomic beam gun F, Fig. 1, described previously,[17] at a collecting voltage of $\sim$10 V. Dosage was monitored by total charge collected. Work function measurements were made after each dose to obtain the work function φ, versus coverage θ, relation. Results are shown in Fig. 2 for silicon (a) and germanium (b). Data on several different silicon surfaces agreed with (a), but in some cases the work function fell less rapidly than shown, as though the cesium did not reach or remain on the cleaved portion of the surface. The germanium curve was taken on only one surface, and the slower drop of φ with θ may be due to this same effect.

Application was carried out at a typical rate of one monolayer in 2h at a vacuum of $\sim2\times10^{-10}$ Torr with the sample at room temperature. The monolayer condition is arbitrarily defined as one cesium ion or atom at each surface site, giving a density of $\sim8\times10^{14}$ cm^2 for the (111) surface of silicon and germanium. This density is reasonable for cesium in the ionic state (ionic diameter=3.38 Å), but somewhat too high for the atomic state, since one monolayer of cesium atoms (atomic diameter=5.40 Å) would contain $\sim4\times10^{14}$ atoms/cm^2 if closely packed.

It was deduced for both silicon and germanium that the sticking coefficient of cesium was quite high at low coverage but dropped to near zero as the monolayer condition was approached. For example, a computed dose of 1.5 to 2.0 monolayers was usually required before work function and photoelectric properties reached the limiting state where they became insensitive to further coverage, interpreted as the "monolayer" condition.

Studies of cesium adsorption on cleaved silicon at room temperature[18] using low-energy electron diffraction indicate that the cesium atoms remain in a disordered state at least during early stages in the monolayer coverage. This disoredered state of the cesium is consistent with the finding that the polarization effect,[8] which exists at clean, ordered silicon and germanium surfaces because electrons are not scattered during emission, disappears as cesium is added.

Both cleaved, and cleaved-and-heated silicon surfaces have been studied during cesium application. The differences in photoelectric emission and work function between the two types of surface[5] disappear gradually during the first half monolayer of cesium, and the covered surfaces of both appear to be the same.

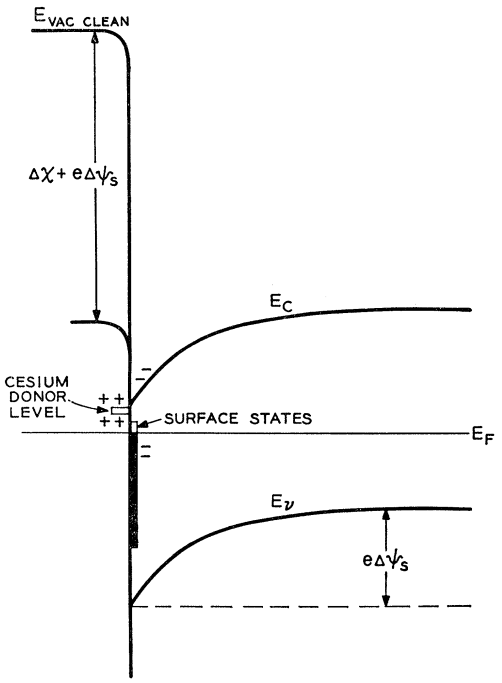

FIG. 3. Action of cesium on silicon and germanium surfaces.

[17] F. G. Allen and G. W. Gobeli, Rev. Sci. Instr. 34, 184 (1963).

[18] J. J. Lander and G. W. Gobeli, J. Appl. Phys. (to be published).

The model that has often been proposed to explain the lowering of the work function of metals and semiconductors by cesium atoms[1,19,20] and which is consistent with the present results, postulates that each cesium atom forms a donor state at or above the conduction band at the surface, see Fig. 3. This is reasonable because the ionization potential of the adsorbed cesium atom will be less than the free atom value of 3.87 eV and thus less than the electron affinity of clean Si, (4.01 eV or clean Ge 4.13 eV).[6] Each Cs atom also presumably annihilates one surface state of the clean surface.

The donor state formed is positive when empty and attracts a negative charge either in the surface states or in the space-charge layer of the semiconductor. The energy bands are thus pulled down at the surface, forcing it to be n type, until the Fermi level lies at or close to the cesium donor level. After this point is reached further cesium atoms produce states that are largely occupied and therefore neutral so that no further band bending occurs. The reduction in work function upon cesium addition can be regarded as the effect of one total surface dipole consisting of the Cs^+ ion outside the surface and its neutralizing electron located in surface states *or* in the space-charge layer. The former contribution lowers the electron affinity $\chi=(E_{vac}-E_c)_{Surf}$. While the latter effect lowers the energy bands inside the surface by $e\Delta\psi_s$, the space-charge potential drop. Since the band bending accounts for less than one-third of the total 3.3 V reduction in work function for silicon and germanium, the change in χ must be the principal effect. It is interesting that the initial slope of the φ-versus-θ curve for silicon [Fig. 2(a)] indicates that each Cs ion changes the average work function by about 20 eV per monolayer—an amount equivalent to the dipole of a monolayer of positive ions placed $\sim$1.6 Å outside their compensating negative charges in a plane conducting surface very much as found by Langmuir[20] and later workers[21] for Cs on tungsten. Heine[22] has shown that this slope is also reasonable for Cs^+ ions on Si if it is assumed that for each ion $\frac{3}{4}$ of one electronic charge, (positive), resides at the ion center 1.6 Å outside the surface, where the dielectric constant is 1, compensated by $\frac{3}{4}$ of one electronic charge, (negative) located on the average 8 Å inside the surface where the dielectric constant is 11.6. A careful analysis of the slope versus coverage of such a plot together with surface structure analysis by low-energy electron diffraction and surface conductivity measurements (see below) should reveal details of the cesium surface interaction which is probably complex. Our results do not permit specification of surface Fermi level position versus coverage, but they do indicate that for both Si and Ge the Fermi level lies near the conduction band for the monolayer coverage.

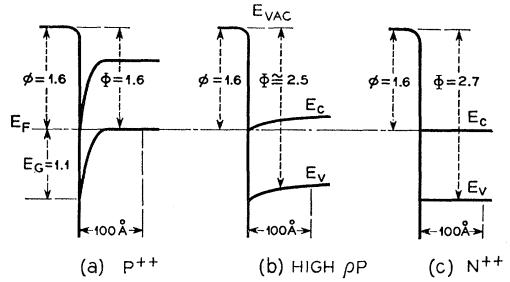

FIG. 4. Approximate surface potential profiles for cesium-covered silicon surfaces. (a) 0.0005 Ω cm p type; (b) 50 000 Ω cm p type; (c) 0.0008 Ω cm n type. A typical escape depth of 100 Å is shown on each.

There is some evidence from the data that the Cs atoms do not form large clusters in the fractional monolayer region. If such clusters occurred, the surface would consist of Cs-covered patches and clean patches, with a work function difference $\Delta\varphi$ of $\sim$3 V. Then whenever the normal collecting field exceeded the patch field of $\sim\Delta\varphi/a$ where a is the patch diameter, each patch would emit independently of the others, and the yield would consist partly of the Cs-covered spectrum with a photothreshold near 1.6 eV, and partly of the clean spectrum. Since such an effect has not been seen in the present work for collecing fields up to $\sim$500 V/cm, clusters of cesium, if present, are smaller than $\sim 50\,\mu$ in diameter. At the collecting fields used, the photothreshold varies smoothly toward lower energy as Cs is added, so that either the cesium atoms do not cluster at all, or else patches are small enough so that the average potential barrier is relatively insensitive to collecting field.

The steepness with which the potential changes normal to the surface as the bands bend down due to the Cs layer will be determined by the bulk-screening length of the sample, i.e., by the doping. Bulk Debye lengths for Si and Ge vary from $\sim$10 Å for heavily doped to 10 000 or 100 000 Å for high-resistivity samples. Approximate potential profiles for three doping levels of cesium-covered silicon typical of samples actually used in this work, based on the solutions of the space-charge equations of Young,[23] or the present authors,[2] are sketched in Fig. 4.

The question remains as to how much photoemission is seen from the cesium layer itself. The yield spectra of six different III-V semiconductors as well as of silicon and germanium, all covered with cesium, have been found to have structure that differs from one semiconductor to the next and yet agrees in detail with structure found in optical reflectivity or absorption measurements made on those same semiconductors with no cesium on the surface. This shows empirically

[19] P. Zalm, Report on 21st Annual Conference on Physical Electronics, MIT, 1961 (unpublished).
[20] I. Langmuir, Chem. Rev. 13, 147 (1933); J. Taylor and I. Langmuir, Phys. Rev. 44, 423 (1933).
[21] J. M. Houston, Advan. Electron. Electron Phys. 17, 125 (1962).
[22] V. Heine, Phys. Rev. 138, A1689 (1965).
[23] C. E. Young, J. Appl. Phys. 32, 329 (1961).

that any cesium emission is weak compared to the bulk emission. Furthermore, as the bulk energy levels in silicon are moved up or down relative to the Fermi level at the surface by varying doping, the energy distributions reflect this change directly (see below) showing that the energy of most emitted electrons is determined by energies in the bulk, not in the surface layer. Finally, if we estimate the probable photoemission from a single layer of cesium atoms, we can show it to be much less than that resulting from the bulk silicon or germanium. Ives and Briggs[24] measured the optical properties of thin layers of cesium. The absorption coefficient, $\alpha=4\pi k/\lambda$, computed from their bulk data extrapolated to one monolayer indicates that cesium could absorb at most $\sim 0.5\%$ of the photons entering the surface with energies between 3 and 5 eV. Not all of this absorption can result in photoemission. Since the measured yields for the cesium-covered surfaces of silicon and germanium range from $\sim 1\%$ near 3 eV to $\sim 10\%$ near 5 eV, expressed in electrons per incident photon, it can safely be said that over most of this range the bulk semiconductor provides at least 80% of the observed photoemission. The Cs monolayer might contribute over 10% of the yield only at photon energies less than 3 eV, and this seems unlikely since the yield for the Cs must fall off near its threshold as does that for silicon and germanium.

III. RESULTS ON SILICON

Surface Fermi-Level Position versus Cesium Coverage

The Fermi level at the surface of clean-cleaved silicon has been placed at 0.23 eV below the midgap,[3] while that of germanium was found to be within a few kT of the valence-band maximum.[6]

Several workers[1,13,25] have assumed that the Cs-covered silicon surface is strongly n type, but the evidence is not yet conclusive. In an effort to determine directly the surface Fermi-level position during cesium application four-point probe measurements were made on cleaved silicon surfaces after successive cesium coverages. Subject to the limitations discussed in the Appendix, the measurements yield the following information. For all three cleavage faces examined of a nominally 50 000 Ω-cm p-type sample, initial V/I values were near 300 000 Ω for the clean surface and rose to a maximum of $\sim 400\,000$ Ω after depositing 0.1 computed monolayer of cesium. (Here, V is the open-circuit voltage across the two center probes while I is the current passed between the two outer ones.) Taking account of a geometric factor arising from the width of the sample (see Appendix), the above increase corresponds to a decrease in surface conductivity of $\sim 0.8\times 10^{-6}$ mhos per square. Beyond 0.1 monolayer of cesium, V/I values fell again but the data were scattered for different samples. The lowest V/I value reached was 11 000 Ω at a computed coverage of ~ 1 monolayer, corresponding to an increase (from the minimum) in surface conductivity of $\sim 100\times 10^{-6}$ mhos per square. It is possible but unlikely that part of this latter increase is due to direct conduction through the cesium layer itself.

From these results we can conclude that: (1) The conductivity of any p-type surface layer initially present on the cleaved silicon surface, including any contribution from surface states was less than 0.80×10^{-6} mhos per square; (2) starting from the clean-cleaved surface, cesium addition moves the surface Fermi-level position first toward the center of the gap then through and away from it. These conclusions are consistent with our proposed model in which the clean-cleaved silicon surface is weakly p type and becomes steadily more n type as cesium ions are added. However, the measured changes in surface conductivity are numerically smaller than our model would predict, if the mobilities at the surface are assumed equal to those in the bulk (~ 500 and 1500 cm^2/V sec for holes and electrons, respectively). Thus, the above conductivity changes would indicate a shift in surface Fermi-level position from 0.18 eV below midgap for the clean-cleaved surface to 0.37 eV above midgap for the cesium-covered surface. Our previously published clean-surface Fermi-level position of 0.23 eV below midgap would produce an initial surface conductance of 3.5×10^{-6} mhos per square for 50 000 Ω-cm silicon, and when enough cesium had been added to move the Fermi level to within 0.1 eV of the conduction band, a surface conductance of $\sim 600\times 10^{-6}$ mhos per square should result. A reduction in surface mobility by a factor of ~ 6 for the cesium-covered surface and ~ 3 for the clean surface would be required to explain the discrepancy between these values and the measured results. The limitations of the four-point-probe technique itself are probably partly responsible here. However, the very low values of surface conductivity for the clean silicon surface are consistent with findings of Handler[26,27] and Heiland,[28] who did not depend on this technique. Conductivity measurements on cleaved germanium surfaces have not been made.

Attempts to determine the Fermi-level position at the surface at intermediate cesium coverage from the difference between the work function ϕ and the extrapolated cube law photothreshold Φ_t were inconclusive, since the yield departed from a definite cube law rapidly as cesium was deposited. It could only be concluded that a definite separation of ϕ and Φ_t values did persist throughout the first 0.2 monolayers of cesium.

Further evidence that the bands were bent down at the surface till the conduction band was at or close to

[24] H. E. Ives and H. B. Briggs, J. Opt. Soc. Am. 27, 395 (1937).
[25] J. A. Burton, Phys. Rev. 108, 1342 (1957).
[26] P. Handler, Appl. Phys. Letters 3, 96 (1963).
[27] P. Handler and D. Aspnes (to be published).
[28] G. Heiland, *Festkörperprobleme* (F. Vieweg & Son, Braunschweig, 1964), Vol. III, p. 147.

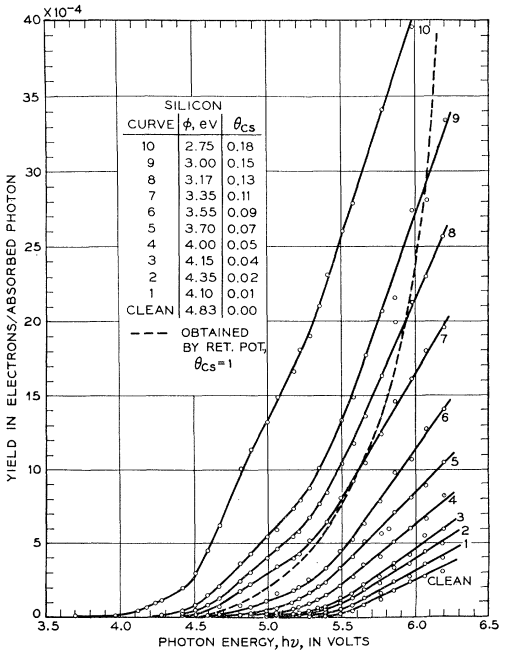

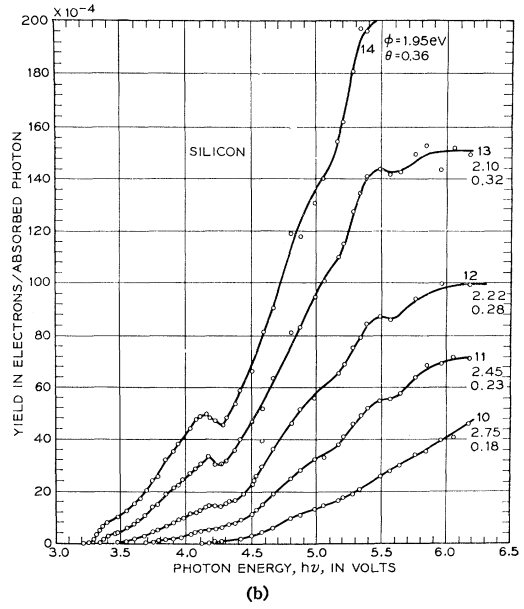

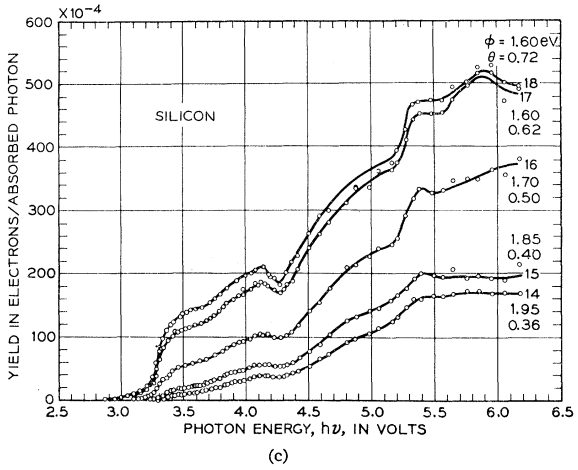

FIG. 5. Spectral yield of 250 Ω cm p-type cleaved silicon at successive cesium coverage. (a) $\theta=0$ to 0.18; (b) $\theta=0.18$ to 0.36; (c) $\theta=0.36$ to $\sim$1.0 monolayers.

the Fermi level with one monolayer of cesium was supplied from yield results at very low photon energies. Both silicon and germanium showed appreciable yield in the cesium-covered condition, at photon energies close to the work function itself $\sim$1.5 eV. This is consistent with emission from filled conduction band states at degenerate n-type surface. The bulk resistivities of both Ge and Si were high so that emission from filled valence or conduction bands in the bulk could be ruled out. Another source of evidence for this degenerate n-type condition of the cesium-covered silicon surface is discussed later where it is shown that the yield curve of high-resistivity silicon is much closer to that of n^{++} type than p^{++} type bulk silicon. Finally, the high-energy edge of the energy distributions (Figs. 9 and 16) shifts downward several tenths of an eV during Cs deposition, which again gives strong evidence that the energy bands at the surface shift downward relative to the Fermi level with Cs addition.

Spectral Yield: Silicon

The yield versus photon energy for successive doses of cesium on 250 Ω cm p-type silicon are shown in Fig. 5 (a), (b), and (c). The yield for the clean surface has

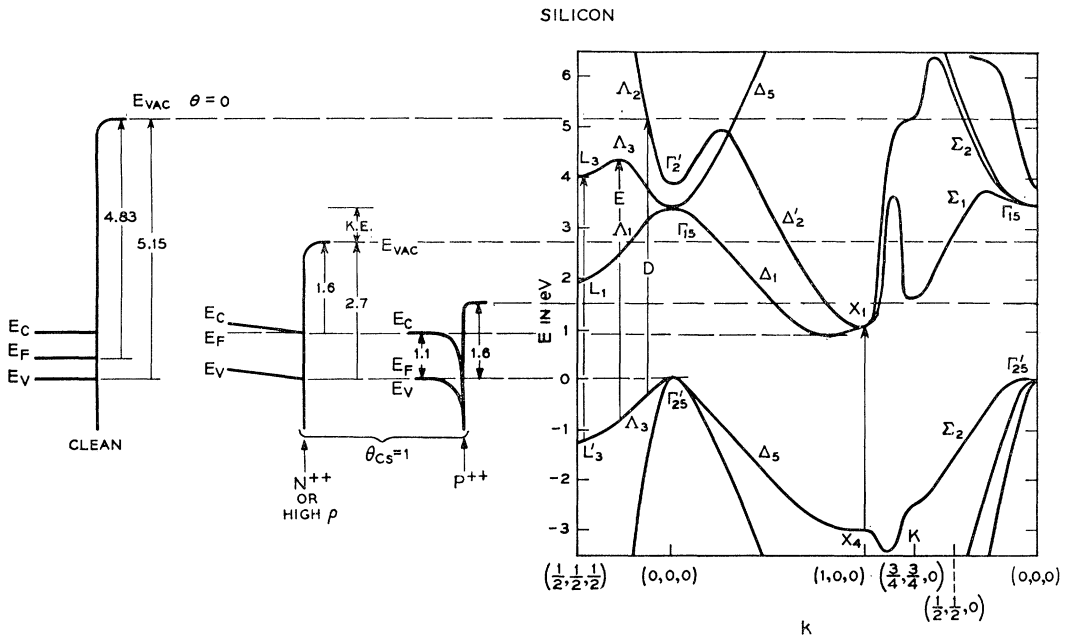

FIG. 6. Energy-versus-k diagram for silicon, after Brust (Ref. 10), showing vacuum level for clean and cesium-covered cases.

been discussed elsewhere.[6] The linear rise above $h\nu = 5.45$ eV is attributed to direct optical transitions followed by escape without scattering, from the Λ region of the upper valence band to the upper conduction band in or close to the [111] direction. This is shown as "*D*" on the *E*-versus-**k** diagram for silicon in Fig. 6 derived by Brust[10] by the pseudopotential method. The curving tail below the linear portion of the clean yield curve is attributed to one or more of several processes that give a higher power law than linear.[6] A cube-law extrapolation of this tail probably gives the location of the valence-band maximum at the surface, while the work function locates the Fermi level at the surface.

A threshold for a direct transition occurs when the "optical energy surface" defined by the equation $h\nu = \xi_1(k) - \xi_2(k)$ is tangent to the "electron energy surface" $E = \xi_1(k)$ with E set equal to the vacuum potential energy. These two surfaces intersect in a point called a "two-dimensional critical point." The locus of these points as E and $h\nu$ are varied describes a line in k space called a "critical line."[29] Every optical energy band has a set of 3 or 4 such critical lines. The symmetry directions Σ and Δ are always critical lines as is Λ when both initial and final states are nondegenerate. Since the upper two valence bands are degenerate in silicon, Λ will not be an important critical line. We attribute the series of one or two straight-line segments into which the curves of Fig. 5(a) seem to be decomposed to a series of one or two distinct direct processes associated with separate critical lines. Though we cannot exclude the possibility that the two processes are from one band it seems likely that they are associated with final states in the upper two conduction bands in Fig. 6. The highest one appears for clean silicon followed by the next lower band when the vacuum potential has been lowered about 1 eV by cesium coverage. However it must be pointed out that the position of these direct photothresholds do not decrease with Cs coverage nearly as fast as predicted from the simple energy-band computations. As more cesium is added the linear portions become curved. This is expected both because the linear relation should hold for only a few tenths eV above threshold[7] and because the cesium, in its disordered state at low coverage, should cause scattering.[8]

Added evidence that the cesium-covered surface emits scattered electrons, while the clean surface emits unscattered electrons was provided by the following experiment. After a full monolayer of cesium had lowered the vacuum level to $\sim$1.5 eV above the conduction-band minimum at the surface, a series of yield-versus-$h\nu$ curves was taken with various fixed retarding potentials applied to the collector surrounding the sample. This is analogous to changing the barrier height with cesium coverage except that the *total* energy of emitted electrons must exceed the externally applied potential barrier, whereas the *normal* energy of the electron incident from inside must exceed the cesium-controlled surface barrier. The entire family of yield-versus-cesium curves could be closely reproduced in this way for all but the nearly clean surface. For this region, the yield curves obtained by the electric retarding potential barrier with the fully cesium-covered surface were *smoothly curved* in contrast to the broken linear curves of the clean surface. The dotted curve in

[29] E. O. Kane (to be published).

TABLE I. Structure in silicon yield.

Photon energy $h\nu$, eV	Feature in Y	Work function when first seen	Feature in reflectivity	Phillips' designation
3.2–3.4	sharp rise	2.1	peak in ϵ_2	$\Lambda_3 \rightarrow \Lambda_1$ or $\Gamma_{25}' \rightarrow \Gamma_{15}$
3.7	dip	2.1		
4.27	sharp dip	2.2	peak in ϵ_2	$X_4 \rightarrow X_1$
4.6–4.9	peak (strong in p^{++})	2.1		
5.2–5.5	shoulder	2.5	hump in ϵ_2	$L_3' \rightarrow L_3$ or $\Lambda_3 \rightarrow \Lambda_3$
5.6–5.8	peak (strong in p^{++})			

Fig. 5(a) shows a yield curve obtained with a retarding potential of ~3 eV applied to a cesium-covered surface and illustrates the contrast in the two forms of curve obtained at approximately the same barrier and yield. The fact that the structure in the yield curves agreed for the two methods at other barrier heights shows once again that the structure in the cesium-covered yield curves is really a function of barrier height, and is not merely an anomalous effect connected with the cesium on the surface.

As the work function is lowered to 2.2 eV, curve 12 Fig. 5(b), a marked jump begins to appear between $h\nu=3.3$ and 4.2 eV, a dip occurs at 4.3 eV and two further humps appear at 4.8 and 5.3 eV. Further cesium doses accentuate these features but do not change their energy location appreciably. The work function values at which these features first appear together with the relevant photon energies are shown in Table I. The exact barrier height from valence-band maximum to vacuum level cannot be specified more accurately than within several tenths of an eV at intermediate cesium coverage.

After Cs dose No. 17, Fig. 5(c), further doses, No. 18 and others, caused little or no further change, so this is assumed to be a "monolayer" condition. At this point the work function measured 1.6 eV, and evidence from the sources cited above indicated that the conduction-band minimum was then close to the Fermi level at the surface. The high resistivity of 250 Ω cm assures that over the maximum escape depth of ~200 Å the bands do not rise inside the surface by more than a few tenths of an eV, so that we have essentially an n-type flat band semiconductor [see Fig. 4(b)]. The barrier height from valence-band maximum to vacuum level for most emitted electrons is then approximately 1.1 +1.4=2.5 eV, where the value 1.4 is taken as the electron affinity must beneath the surface where the bands have bent upward ~0.2 eV from their position at the surface.

Theoretical Yield for Silicon

In Fig. 7(a) we have shown again the yield for the cesium-covered surface of 250-Ω cm p-type silicon and in addition the dotted curve shows a calculated theoretical yield curve for silicon. This was obtained by Brust, Cohen, and Phillips[9] by a machine summation of yield contributions from 50 000 points in the Brillouin zone of the E-versus-$\mathbf{k}$ diagram (Fig. 6). In the initial calculation, direct transition with constant matrix elements and escape of all electrons with upper states $E_1(k)>E_{\text{vac}}$ were assumed, and a strong resemblance between experimental and calculated yields was already evident for the whole family of different barrier heights. Brust[30] then refined the calculation, using a finer mesh, and assumed first, that electrons were emitted with no scattering, that is, conserving the momentum vector $\mathbf{k}$ of the upper state $E_1(\mathbf{k})$ into which they were excited; and second, that they were completely scattered in the upper state. He then computed the probability of escape, $P(E_1,k)$ for each transition in the unscattered case as

$$P(E_1,k)=1 \quad \text{if} \quad E_1(\mathbf{k})>(\hbar/2m_0)k_t^2+E_{\text{vac}}$$
$$=0 \quad \text{otherwise}, \qquad (1)$$

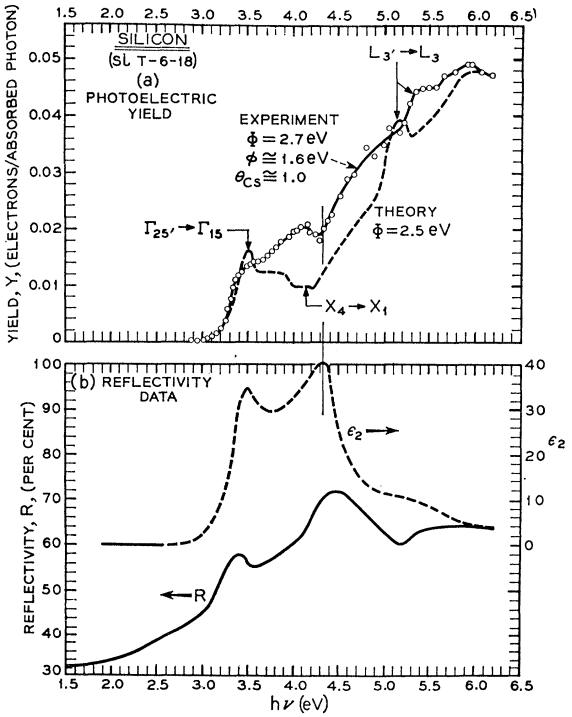

FIG. 7. Yield and reflectivity of silicon. (a) Comparison of experimental yield for 200 Ω cm cleaved silicon covered with cesium with theory of Brust. (b) Reflectivity and ϵ_2 results of Philipp and Taft (Ref. 32).

[30] D. Brust, *Proceedings of the International Conference on the Physics of Semiconductors, Paris, 1964* (Academic Press Inc., New York, 1965). Also, Phys. Rev. **139**, A489 (1965).

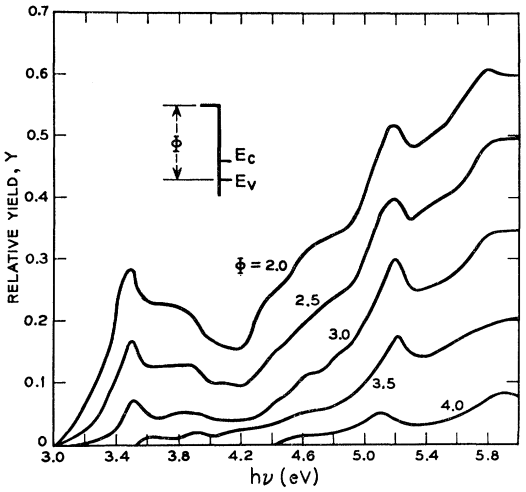

FIG. 8. Theoretical yield curves for silicon at different barrier heights Φ, after Brust (Ref. 30).

where k_t is the component of k parallel to the surface and m_0 is the free-electron mass. For the scattered case, Brust computed the escape probability as a function of upper state energy $P(E_1)$ by averaging $P(E_1,k)$ given by (1) over all **k** values in the upper state.

Since a monolayer of cesium is known to cause momentum scattering,[8] however, a more accurate calculation would include randomization of k_t upon crossing the surface. Since the energy level structure at the surface cesium layer is unknown, this approach cannot be followed through and Brust's assumption is probably the best one can do at present.

Note, however, that no depth dependence of emission or energy losses were introduced by Brust. These energy-loss effects could be partially taken into account by multiplying Brust's calculated distributions by an energy-dependent escape probability which would act to reduce preferentially emission of high-kinetic-energy electrons due to the strong energy dependence of pair production.[31]

Another effect which may alter the structure of the computed distributions is the dependence of escape probability on the group velocity of the final state. In regions of high state density which are responsible for the peaks in Brust's calculated yield and energy distributions the group velocity is low. At high KE, when the pair-production length is shorter than the phonon-scattering length, the group-velocity effect suppresses peaks in velocity distributions which arise because of high electron-state densities. At lower KE where the converse is true, the electrons may lose smaller amounts of energy and thereby "dribble" into regions of higher group velocity (higher escape probability). This will act to shift peaks from computed positions to lower energies. The only way this effect could be taken into account would be by a complete Monte Carlo calculation of escape trajectories using the energy dependence of pair production[31] which was unavailable at the time of Brust's original calculation.

Brust found that the model with scattering gave better agreement with experiment, though the structure was not drastically changed by the escape assumptions. The dotted curve in Fig. 7(a) shows his results for a barrier height Φ from the valence-band maximum to E_{vac} of 2.5 eV with the ordinate arbitrarily matched to fit the experiment at 6.2 eV. While the agreement is not perfect, the principal features of the experimental curve are matched by the theory. Figure 8 shows a family of Brust's computed yield curves for different barrier heights. These show a good over-all resemblance to experimental yield curves at successive cesium coverage, Fig. 5.

One discrepancy between theory and experiment lies in the fact that the experimental yield at high photon energies (6.0 eV) increases by a much larger factor (300%) upon lowering the barrier from 3.0 to 2.7 eV [lowering the work function from 1.9 to 1.6 eV, curves 14 to 17, Fig. 5(c)] than does that of the theory (20%). This suggests that energy-loss mechanisms are important in the experiment and provide a large supply of electrons at low kinetic energies that can escape at low barrier heights. This conclusion is also borne out in the energy distributions and will be discussed later.

Reflectivity of Si

The reflectivity of Si taken by Philipp and Taft[32] is shown plotted below the yield curve, Fig. 7(b). Also shown is the imaginary part of the dielectric constant ϵ_2, proportional to the joint density of states, derived from the reflectivity by the Kramers-Kronig relation. The principal features in the yield and reflectivity data for silicon with the probable direct transitions involved are summarized in Table I.

Energy Distributions—Silicon

The kinetic energy of an emitted electron gives its energy above the vacuum level, E_{vac}. The work function φ is the energy from the Fermi level E_F to the vacuum level E_{vac} (see Fig. 6). If the Fermi level lies above the valence-band maximum by E_F-E_V, the barrier Φ for emission from the valence band is

$$\Phi=\varphi+E_F-E_V. \tag{2}$$

The energy of an emitted electron above the valence-band maximum is then

$$E-E_V=\text{KE}+\Phi. \tag{3}$$

Since, for semiconductors, the bands normally bend up or down near the surface, one must determine an *effective* barrier Φ_{eff}, at a depth where most electrons originate. To do so, we determine the band positions in

[31] E. O. Kane (to be published).

[32] H. R. Philipp and E. A. Taft, Phys. Rev. **120**, 37 (1960).

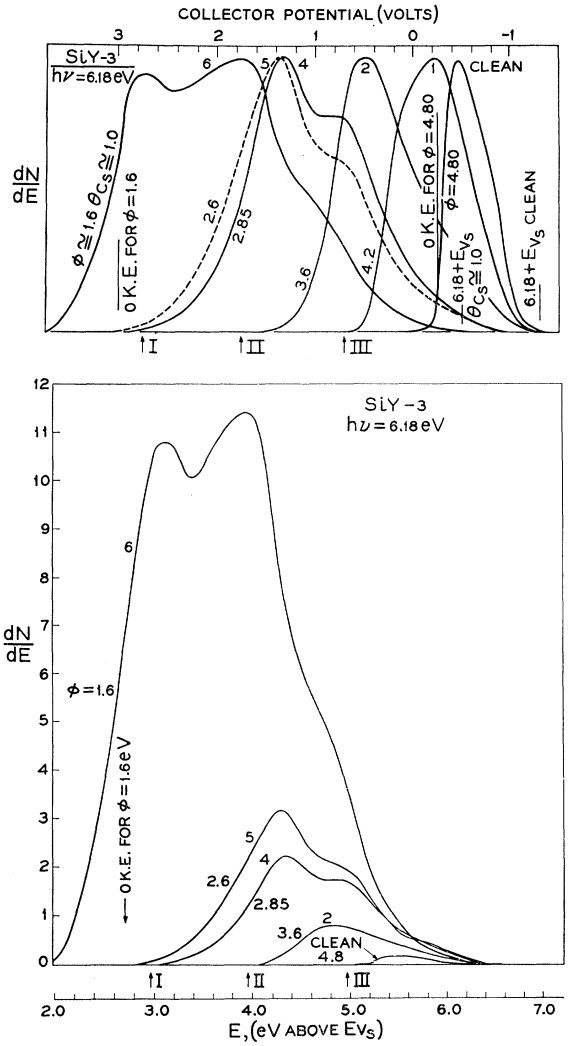

FIG. 9. Energy distributions from 200 Ω cm p-type silicon at successive cesium coverages at $h\nu=6.18$ eV. (a) All curves plotted versus the potential applied to the collector and normalized to the same heights. (b) Energy scale relative to the valence-band maximum at or near the surface, E_{Vs}, determined by Eq. (4), distributions shown with area of each proportional to yield.

bulk and surface relative to the Fermi level, compute the space-charge profile and then compare these with typical escape depths of electrons $-\sim 20$ Å for clean surfaces and ~ 150 Å[1] for cesium-covered surfaces. Two general cases arise: (1) For high-resistivity bulk, band bending is gradual over depths of ~ 150 Å so that an essentially flat band condition prevails. E_F-E_V and thus Φ are approximately constant over the escape depth, and will be equal to their values at the surface, regardless of where the surface Fermi level is pinned (near midgap for clean silicon, near E_V for clean germanium, or near E_C for cesium-covered silicon and germanium). (2) The second case is that for very highly doped material where space-charge band binding is complete within 10 or 20 Å of the surface. For cesium-covered surfaces nearly all electrons then originate from beneath the space-charge region. Hence, the effective barrier Φ is one energy gap less for p^{++} bulk than for n^{++} bulk or high-resistivity bulk, as is illustrated in Figs. 4 and 6. We define the valence-band maximum at the point where most electrons originate as E_{Vs}. This will be equal to the valence-band maximum at the surface for high-resistivity samples.

Distributions in total energy of electrons emitted from clean-cleaved (111) silicon surfaces have been presented previously.[5,6] At $h\nu=6.18$ eV there is a high-energy shoulder added to the principal lower energy group, while at 5.63 eV only a single group remains. The principal group at 6.18 eV (which gives rise to the linear rise in yield with $h\nu$), was attributed to electrons resulting from a direct transition from the Λ_3 region of the upper valence band to the Λ_2 region of the upper conduction band. The high-energy shoulder (corresponding to the curved tail in yield), is attributed either to indirect transitions from the maximum of the valence band, to transitions from the valence-band maximum with normal momentum exchange with the surface, or possibly to emission from filled surface states.

As cesium is added, the energy distributions change dramatically. Results for silicon at one photon energy, 6.18 eV, showing the changes produced by successive cesium coverage, are given in Fig. 9. The measured experimental abscissa for all curves was collector potential, shown at the top. The energies E relative to the valence-band maximum may be obtained as follows: The value of $(E_F-E_V)_S$ changes from its value of 0.32 eV for the clean surface to 0.55 eV (midgap) at $\theta_{Cs}=0.1$ monolayer as deduced from surface-conductivity measurements. *Assume* a uniform surface-state density throughout E_G and therefore that the rate of change of $(E_F-E_V)_S$ with respect to θ is approximately constant. Then the Fermi level will have reached the conduction-band edge $(E_F-E_V)_S=1.1$ eV at $\theta\cong 0.35$. From Fig. 2 of φ versus θ and the measured work function of the Si for each of the distributions shown in Fig. 9(a), it is possible to correct the raw data of Fig. 9(a) so that all curves can be plotted on the horizontal axis with energies relative to E_V, i.e.,

$$(E-E_V)_S=E_{\text{meas.}}+(\Phi_{\text{coll}}-\Phi_{\text{Si}})_\theta+(E_F-E_V)_{S,\theta}. \quad (4)$$

Figure 9(b) shows the data of Fig. 9(a) normalized such that the area of each distribution is proportional to the yield and with the electron energies plotted relative to the valence-band edge of Si as indicated above.

As cesium is added, the vacuum level is lowered through the upper states carrying with it the probability of escape function which forms a lower energy envelope for all curves. When this envelope has exposed a peak in the distribution and passed to lower energies, a true peak due to band structure should remain at a fixed location on this diagram. This behavior is seen for two definite peaks, labeled II and III in Fig. 9. Peak I, at

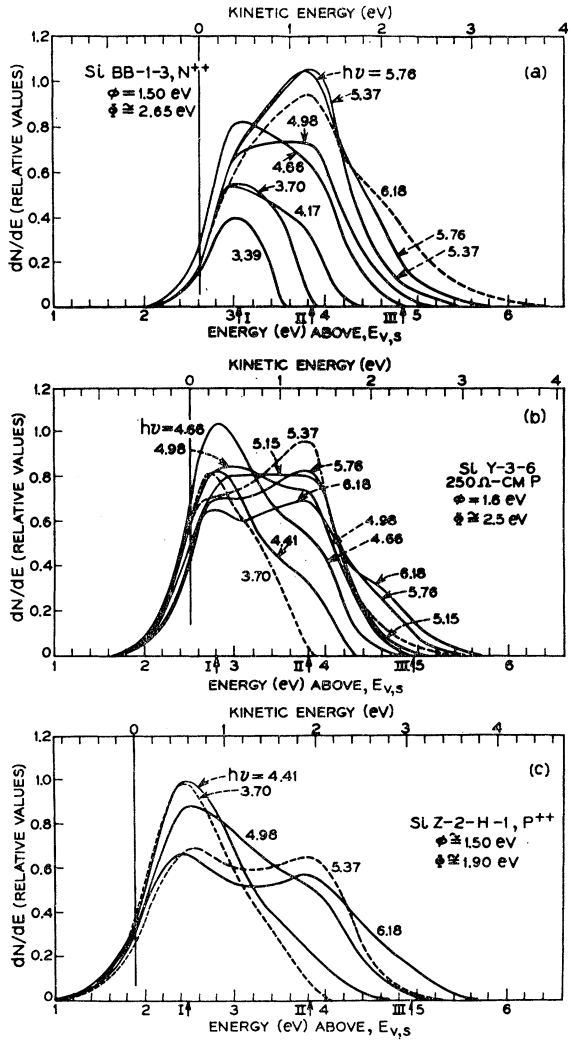

FIG. 10. Energy distributions from silicon covered with one monolayer of cesium at various photon energies. Energy scales show true kinetic energy and energy relative to valence-band maximum at or near the surface, E_{Vs}. (a) 0.005 Ω cm n type; (b) 250 Ω cm p type; (c) 0.0008 Ω cm p type.

lowest KE, is not definitely located since the vacuum level has not passed far enough below it to be sure its position is not still affected by the escape envelope.

Note that in Fig. 9(b), each curve of higher Cs coverage exceeds that of all lower Cs coverages, since the yield at all kinetic energies is increased by lowering the barrier. Note also on Fig. 9(b) the very large increase in area under the low-energy peak caused by a slight decrease in barrier height as the work function φ is reduced from 2.6 to 1.6 eV.

The significance of any one peak at a given energy on this diagram is that electrons excited by 6.18-eV photons from lower to upper states in the crystal, have a preferred probability of emission at that energy. If direct transitions with no energy loss during emission are involved, the energy of each peak gives the energy of a high-density group of upper (empty) states in the crystal lying just $h\nu$ above a high-density group of lower (filled) states at that same k vector.

Such direct transitions with no energy loss should in general give rise to peaks which move in KE as the photon energy $h\nu$ is changed. This is because the upper energy surface that satisfied $h\nu=\xi_1(k)-\xi_2(k)$ over a range of $h\nu$ is not in general flat on the E-versus-$\mathbf{k}$ diagram. Figure 10(b) shows the total energy distributions for a family of *different* photon energies for a fully cesium-covered (111) cleaved surface of 250 Ω cm p-type silicon. The dN/dE values are shown in their true relative heights. Energy scales showing ture KE and energy relative to the valence-band maximum are included. The same three peaks seen previously in Fig. 9 at $h\nu=6.18$ eV are identified again here. Note that the nonideal geometry discussed in the Appendix smears the low-energy end of the curves below zero KE. When approximate corrections are made for this the low-energy peak is raised in height by 10 to 20% relative to the rest of the distribution.

Since the lowest energy peak I could be due to electrons whose energy has been degraded, we hesitate to attribute it to band structure. The relative yield of these low-energy electrons (area under peak I) is seen to rise to a maximum as $h\nu$ increases from 3.70 to 4.66 eV, and then to fall again steadily with rising $h\nu$ up to 6.18 eV, the end of the presently available photon range.

Part II, well resolved for all $h\nu>4.41$ eV, rises to a maximum yield at ~5.37 eV and then falls at higher photon energies. Its location on the energy axis remains surprisingly constant, any movement at all being less than 0.1 eV as $h\nu$ varies from 4.4 to 6.18 eV.

Peak III, from Fig. 9, which is seen as a high-energy shoulder in Fig. 10(b), is present for $h\nu>4.98$ eV, and increases in yield steadily through 6.18 eV. It is difficult to say whether its KE location moves with $h\nu$; it may move upward by a few tenths eV, but not more, as $h\nu$ increases from 4.66 to 6.18 eV.

Band-Bending Effects on Yield and Distributions from Silicon

As bulk doping is changed from n^{++} to p^{++} the surface Fermi level for the cesium-covered surface remains clamped near the conduction band and the energy bands beneath the surface move up relative to the vacuum level by one energy gap, 1.1 eV for silicon. This reduces the barrier height for most emitted electrons from 2.7 to 1.6 eV (see Fig. 4). It should thus greatly increase the yield and shift kinetic energies of true peaks upward by 1.1 eV.

The experimental yield curves for a degenerate p-type (0.0008 Ω cm) and a degenerate n-type sample (0.0005 Ω cm) covered with a monolayer of cesium are shown in Fig. 11(a) and (c), for comparison with the 250 Ω cm yield, Fig. 11(b). It is seen that the yield is about

three times as high for the p^{++} type bulk as the n^{++} type bulk at $h\nu=6.0$ eV, and about eight times at 3.6 eV. The fact that the yield of the nearly flat-band (250 Ω cm p-type bulk) is much closer in magnitude and structure to the n^{++} type than to the p^{++} type curve is evidence that the surface in all cases is clamped strongly n type by cesium. The argument for this is given in the Appendix.

Scheer and Van Laar's results agree qualitatively with the present work, though most of the structure discussed here was not resolved in their experiments. Spicer and Simon[13] published yield curves for a highly p-type bulk silicon crystal covered with cesium, which again agree qualitatively with these results but show less structure. The sharp peak seen by them at 3.7 eV was not found here, though it was carefully sought using a p-type crystal of 0.0008 Ω cm (10^{20} cm^{-3}). Since this sample gave a somewhat larger absolute yield than theirs it was presumably even *more* p-type than their sample, so that the absence of the peak cannot be attributed to insufficient band bending.

The effect of change in bulk doping upon energy distributions from cesium-covered silicon is shown in Fig. 10(a) and (c) where the results for degenerately n- and p-type bulks may be compared with the case of the 250 Ω cm sample [Fig. 10(b)]. The energy distributions for the three dopings have been aligned vertically not by kinetic energy but by the energy E relative to the valence-band maximum in the crystal (lower scale). This causes peaks due to bulk band structure to align vertically in the three cases, while the kinetic energy zero moves to the left in going to p^{++} bulk. The energy scales for Fig. 10(a) and (b) were derived directly from work function data. For the p^{++} sample, Fig. 10(c), for which the band-bending effects on KE should be most severe, the energy scale was located more reliably by aligning peak II directly below that for Fig. 10(b). This involved a shift of ~0.4 eV from the result obtained assuming infinitely sharp band bending, and implies that most electrons escaped from a point in the space-charge region where the valence band was still ~0.4 eV below the Fermi level. From Fig. 4(a), this distance is ~30 Å beneath the surface, which is consistent with our earlier findings[2] for the high photon energies ($h\nu>4.4$ eV) that give peak II.

The fact that the lowest energy peak I occurs at approximately the same *kinetic energy* for all three samples but at different energies relative to E_{Vs}, confirms that this is not a "true" peak where energy is determined by bulk band structure. Also, when the distributions in 10(a), (b), and (c) are normalized correctly relative *to each other* the area under peak I is about eight times higher for the p^{++} than the n^{++} sample, at corresponding $h\nu$ values. From this it follows that it cannot be of purely surface origin, since the work function of all cesium-covered samples was ~1.6 eV. Peak I must thus arise from a supply of electrons from the bulk ranging in energy from 3.6 eV above the valence-band edge and extending downward with rapidly increasing density. They could either be degraded from higher states, or could arise from a peak that is just below the escape envelope for p^{++} samples.

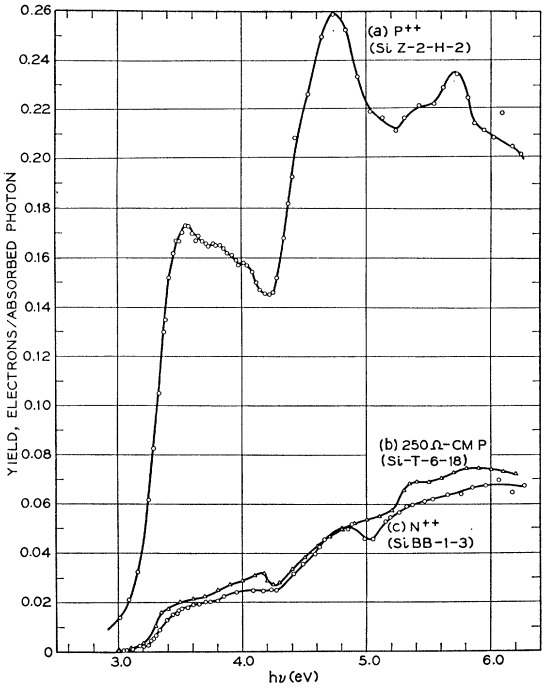

FIG. 11. Dependence of spectral yield of cesium-covered silicon upon bulk doping; (a) 0.0008 Ω cm p type; (b) 250 Ω cm p type; (c) 0.005 Ω cm n type.

Peaks II and III, on the other hand, do move up in KE by approximately 0.8 eV in going from n^{++} to p^{++} as predicted for true peaks. It is interesting to note that an upward shift in peak location of ~0.2 eV in KE occurs between the n^{++} and the 250 Ω cm sample. While the band bending is gradual for this high a resistivity, it is fast enough near the surface to raise the average potential at the origin of the emitted electrons by this much over the n^{++} case, see Fig. 4(b).

Spicer and Simon[13] published energy-distribution curves for cesium-covered silicon. They observed only two peaks, which correspond to our I and II, and reported that peak I moved with increasing $h\nu$ for low photon energies. When the distribution curves are normalized according to yield, the low-energy side is seen to fall inside a common envelope determined by the probability of escape. The apparent movement of the low-energy peak is probably strongly influenced by this escape envelope as yield increases with photon energy. Thus, we feel that the designation of peak I as a prominent feature of the band structure of silicon is questionable.

More recently Eden and Spicer[33] have analyzed the yield spectrum and velocity distributions from Cs-

[33] R. C. Eden and W. E. Spicer (to be published).

TABLE II. Features of kinetic-energy distributions for Cs-covered silicon, $\varphi \cong 1.5$ eV.

Peak number	Kinetic energy, eV n^{++}	250 Ω cm p	p^{++}	Upper-state energy above $E_{V,S}$ n^{++}	250 Ω cm p	p^{++}	$h\nu$, eV Range	Max. yield at	Phillips' designation Transition
I	0.40	0.28	0.60	3.05	2.80	2.48	All $h\nu > 3.17$	4.66	$\Lambda_3 \rightarrow \Lambda_1$ and degraded electrons
II	1.25	1.3	1.95	3.85	3.80	3.80	All $h\nu > 4.17$	5.37	
III	2.25	2.45	3.10	4.85	4.95	4.95	All $h\nu > 5.37$	>6.27	$\Lambda_3 \rightarrow \Lambda_3$

covered silicon in terms of "nondirect" transitions. They assume that conservation of **k** vector of the initial and final states is not important and rather that the absorption of photons depends only on the product of the initial- and final-state densities as a function of energy. Their computations yield excellent agreement with the observed velocity distributions. However, this assumption leads to no structure in the yield apectra such as is observed in Fig. 5, and it seems clear that such structure must arise from a direct transition mechanism in which **k** conservation is important. The results of Spicer and Eden indicate that a fraction of the photoelectric yield *might* be due to "nondirect" transitions which underlay the direct transtitions.

However, Gobeli, Kane, and Allen[34] have demonstrated that careful accounting for the excited-electrons escape depth greatly improves the agreement between experimental velocity distributions and the theoretical calculations of Brust which are derived on the basis of a direct excitation. Kane[31] has further taken into account the effects of group velocity on the escape probability and the effects of energy degradation. His work together with this present work and that of Ref. 34 indicates that the photoelectric properties of Cs-coated Si are substantially accounted for on the basis of a direct transition theory. The features of the kinetic energy distributions from cesium-covered silicon are summarized in Table II.

Interpretation and Assignment of Structure for Silicon

Referring to the yield, reflectivity and energy distribution data simultaneously we can say the following in relating these to the E-versus-**k** diagram, Fig. 6.

(1). The sharp rise in yield at 3.2 to 3.4 eV corresponds to the peak in both R and ϵ_2 near 3.5 eV. The resulting electrons are emitted at low KE in peak I or at an energy E of 2 to 3 eV above the valence-band maximum at $\Gamma_{25'}$. This feature is not inconsistent with direct transitions near $\Lambda_3 \rightarrow \Lambda_1$ or $\Gamma_{25'} \rightarrow \Gamma_{15}$ which would supply the high yield as well as the large range of KE observed. Such an assignment has been suggested earlier from both photoemission[13] and reflectivity[11] results.

(2). The strong dip in yield at 4.25 eV corresponds to the peak in R and ϵ_2 near 4.4 eV, and has no corresponding feature in the distributions. This is consistent with excitation to a final state having a low escape probability, such as, for states lying close to or below the vacuum level at all work functions, i.e., $E < 1.6$ eV. It can probably be attributed, at least in part, to $X_4 \rightarrow X_1$ transitions, again in agreement with earlier work.[13,26] The possible effect of a "dead layer" at the surface when bands bend up sharply beneath the surface and optical absorption increases suddenly near a given $h\nu$ will be discussed later in connection with this dip.

(3). The most prominent feature of the energy distributions is peak II at $E = 3.8 \pm 0.1$ eV. It remains surprisingly constant in energy as $h\nu$ varies, but Brust's[30] calculated energy distributions, Fig. 12, based only on direct transitions, do show just such a prominent peak at $E \cong 4.3$ eV, which varies only ~ 0.3 eV in position

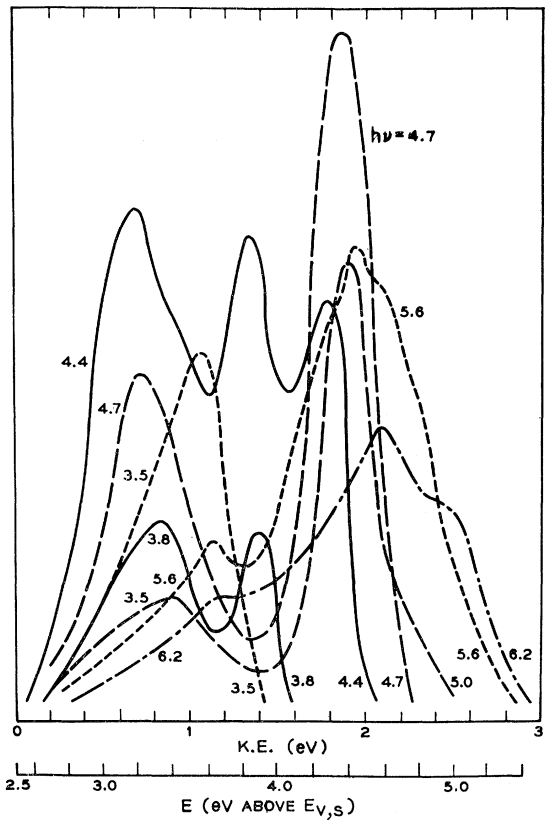

FIG. 12. Energy distributions for silicon computed by D. Brust (Ref. 30). The vacuum level is taken 2.5 eV above the valence-band maximum.

[34] G. W. Gobeli, E. O. Kane, and F. G. Allen, Proceedings of the International Colloquim on Optical Properties and Electronic Structure of Metals and Alloys, Paris, 1965 (to be published).

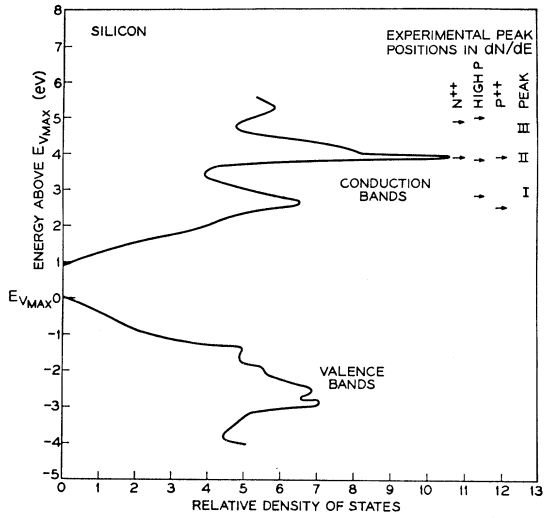

FIG. 13. Density of states in silicon computed by Kane (Ref. 31). Shown on the right are the locations of the experimental peaks in energy distributions found in this work.

between $h\nu=4.4$ to 6.2 eV. This peak is due to a sharp maximum in Brust's conduction-band density of states at 4.3 eV. Kane's[31] calculated density of conduction-band states, Fig. 13, starting with somewhat different parameters than Brust, and including one more valence band, also shows this sharp peak but it occurs slightly lower at 3.9 eV. Clearly the experimental peak II is closely related to that predicted in both Brust's and Kane's calculations.

However, because of the group-velocity effect on the escape probability and thus on peak positions in energy distributions discussed above, we do not expect that such peaks accurately locate state-density maxima. However, from a purely experimental standpoint this characteristic peak in both KE distributions and density of states can serve as a reference level in future studies. Judging by increments in areas under the distributions near $h\nu=4.7$ eV, electrons emitted in peak II cause the shoulder in the yield curves from 4.6 to 4.9 eV, Fig. 11.

The fact that the theoretical energy distributions of Brust show far more fine structure at low photon energies than do the measured ones for silcion is partly to be expected from phonon losses. These become appreciable below 4.0 eV electron energy. They will shift peaks to somewhat lower energy and smear them out increasingly as $h\nu$ decreases.

(4). The shoulder on the yield curve between 5.2 and 5.5 eV corresponds to the slight peak in R and ϵ_2 near 5.4 eV, and probably produces electrons in peak III of the distributions at $E\cong 4.8$ eV. $L_{3'}\rightarrow L_3$ or $\Lambda_3\rightarrow\Lambda_3$ transitions could satisfy the range of photon and kinetic energies required. In identifying the transitions responsible for structure, however, caution must be exercised. Recent calculations of Kane[29] have shown, for example, that the peaks in joint density of states in Si at 4.3 and 5.3 eV [see Fig. 7(b)] cannot be simply ascribed to X and L transitions. They involve several other regions in the Brillouin zone whose contributions are *larger* than those from X and L. Hence the only safe procedure in the future, for identifying structure with the energy band diagram, will be to match experimental results with a computation of contributions from throughout the whole Brillouin zone.

IV. RESULTS ON GERMANIUM

Spectral Yield of Germanium

The spectral yield of clean-cleaved (111) germanium surfaces has been presented previously.[6] As discussed, the Fermi level is believed to lie at or near the valence-band maxima of the cleaved germanium surface. As cesium is added, the work function is lowered as shown in Fig. 2(b), where the x axis is the computed coverage assuming that one monolayer has $\sim 8\times 10^{14}$ atoms/cm^2.

The yield of a (0.3 Ω cm) p-type germanium surface for successive cesium coverages is shown in Fig. 14. The two linear portions of the clean-surface change to

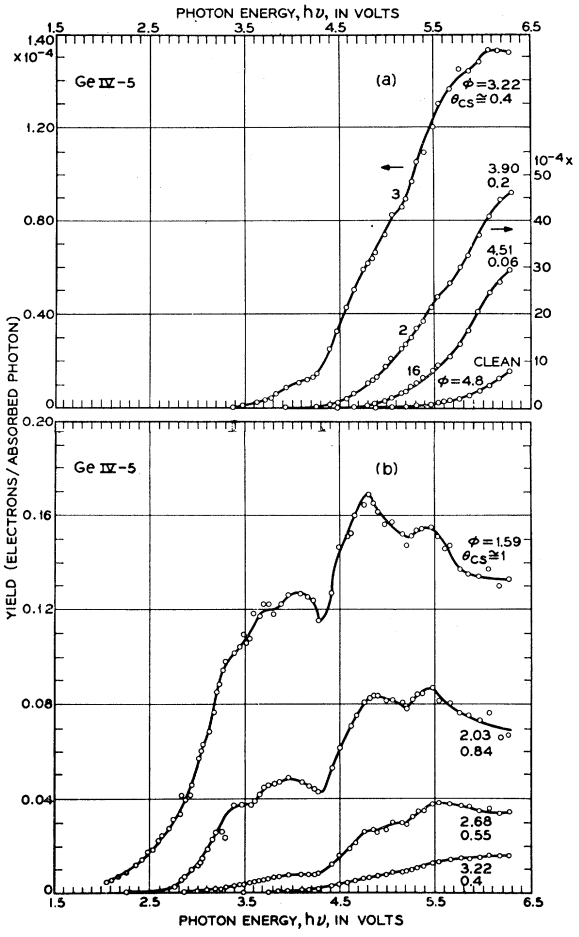

FIG. 14. Spectral yield of 0.3 Ω cm p-type cleaved germanium at successive cesium coverages. (a) $\theta_{Cs}=0$ to 0.4; (b) $\theta_{Cs}=0.4$ to ~1.0.

TABLE III. Structure in germanium yield.

Photon energy $h\nu$, eV	Feature in Y	Work function when first seen	Feature in reflectivity	Phillips' designation
2.35	dip	1.5	peak in ϵ_2	
2.9–3.2	sharp rise	2.7	dip in R	$\Gamma_{25'}^{3/2} \rightarrow \Gamma_{15}$
3.6	fine structure	2.7	weak peak in ϵ_2	$\Gamma_{25'}^{1/2'} \rightarrow \Gamma_{15}$
4.3	sharp dip	3.2	sharp peak in ϵ_2	$X_4 \rightarrow X_1$
4.4–4.8	sharp rise	2.6		
5.4–5.5	peak	3.2	weak peak in ϵ_2	$L_{3'} \rightarrow L_3$

a continuously rising curve after a coverage of ~0.2 monolayers. Definite structure in the yield curve becomes apparent when the work function has been lowered to ~3.2 eV, consisting of a sharp dip at $h\nu$ =4.3 eV, a hump at ~4.8 eV and a second dip at 5.2 eV. (Alternatively, the latter dip could be interpreted as the onset of a sharp new rise.) At this work function of 3.2 eV, about 0.4 of a computed monolayer of cesium has been added, and the vacuum level lies between ~3.2 and ~3.9 eV above the valence-band maximum at the surface.

As cesium coverage continues and work function drops below 2.5 eV, a sharply rising shoulder develops starting near $h\nu \cong 3.0$ eV and fine structure appears at ~3.6 eV. The other structural features persist and become more pronounced until the monolayer condition is reached at a work function of ~1.6 eV. The dip at 4.3 eV becomes particularly sharp. Yield at energies above 5.4 eV actually drops off increasingly relative to the peak yields at 4.8 and 5.4 eV.

At full cesium coverage, a very low-energy minimum is seen at ~2.35 eV, which then merges smoothly with the sharp rise at 3.0 eV. These structural features are summarized in Table III.

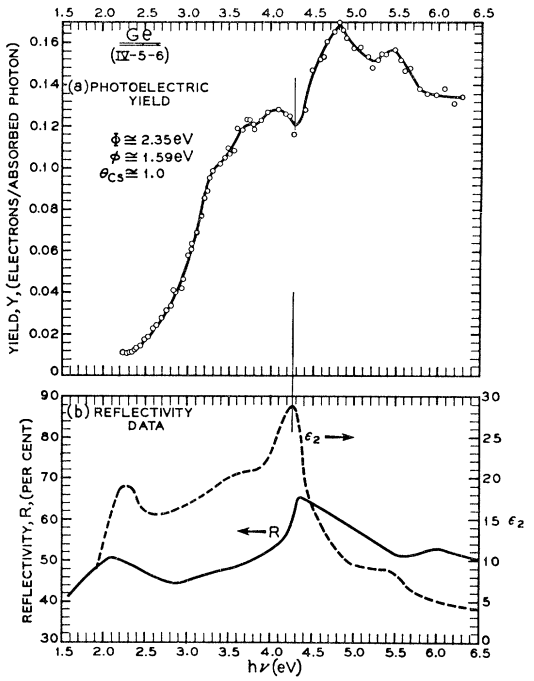

FIG. 15. Yield and reflectivity of germanium. (a) Photoelectric yield of cesium-covered surface; (b) reflectivity results of Philipp and Taft (Ref. 35) and derived ϵ_2 values (Ref. 29).

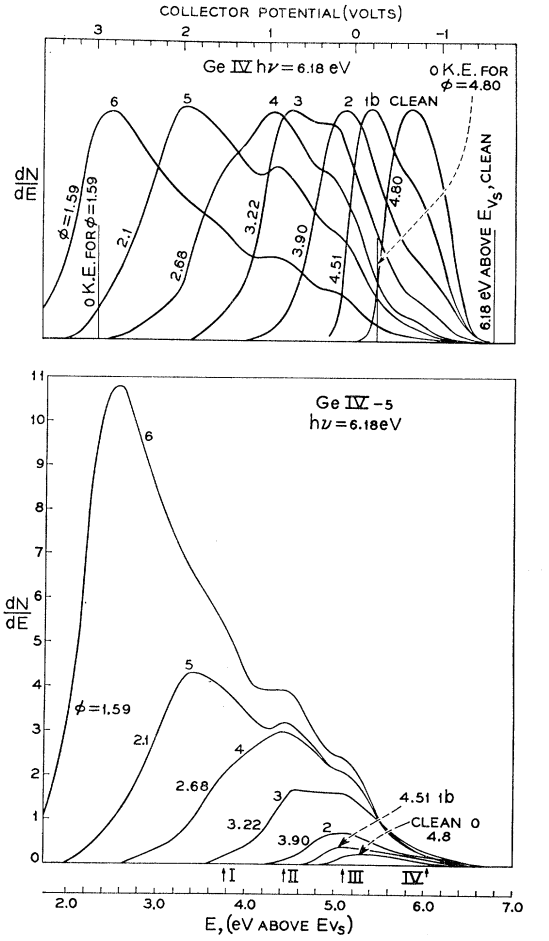

FIG. 16. Energy distributions from germanium at successive cesium coverages at $h\nu$=6.18 eV. (a) All curves plotted versus the potential applied to the collector and normalized to same heights. (b) Energy scale relative to the valence-band maximum at or near the surface $E_{V,S}$, determined by Eq. (4), distributions shown with area of each proportional to yield.

Reflectivity of Ge

The reflectivity data of Philipp and Taft[35] for germanium is shown below the yield curve for cesium-covered germanium in Fig. 15(b). Again, the derived values of ϵ_2[36] as well as the R data are shown. It is seen that there is a definite correlation between the yield and reflectivity data in the structure at 2.3, 3.5, 4.27, and 5.4 eV.

[35] H. R. Philipp and E. A. Taft, Phys. Rev. 113, 1002 (1959).
[36] M. P. Rimmer and D. L. Dexter, J. Appl. Phys. 31, 775 (1960).

TABLE IV. Features of kinetic-energy distributions for Cs-covered germanium, $\varphi \cong 2.0$ eV.

Peak number	Kinetic energy, eV	Upper-state energy above $E_{V,S}$	$h\nu$, eV Range	$h\nu$, eV Max. yield at	Phillips' designation
I	$1.0 \rightarrow 1.3 \rightarrow 1.0$	$3.75 \rightarrow 4.1 \rightarrow 3.7$	$3.39 \rightarrow 6.18$	4.98	$\Gamma_{25'} \rightarrow \Gamma_{15}$
II	$1.5 \rightarrow 1.7$	$4.2 \rightarrow 4.45$	$4.17 \rightarrow 6.18$	5.76	$L_{3'} \rightarrow L_3$
III	2.43	5.18	$\geqslant 5.76$	>6.18	Σ
IV	3.3	6.10	$\geqslant 6.18$	>6.18	Σ

Energy Distributions from Germanium

Total energy distributions for clean-cleaved Ge(111) faces, previously published,[6] show two distinct groups of electrons at $h\nu \geq 5.82$ eV, but only one at lower photon energies, and this behavior correlates well with the two direct transitions postulated. The energy distributions at one photon energy, 6.18 eV, at successive cesium coverages for a cleaved germanium surface are shown in Fig. 16. The data plotted with energies measured both by the collector potential, and relative to the valence-band maximum just below the surface, $E_{V,S}$. Figure 16(a) shows all curves normalized to the same height while 16(b) shows them in their true relative height, after the low coverage distributions were shifted horizontally according to Eq. (4) as done for the silicon data.

As for the case of silicon but in even more pronounced form here, peaks are uncovered as the vacuum level is lowered, which then remain fixed in energy as the vacuum level moves below them. At least four such peaks are seen for the fully covered surface. The location of all peaks, including I here, seems definite since in each case further vacuum level lowering has left the peak positions unchanged. Again, as for silicon Fig. 14(b) shows that all lower Cs curves fall within the higher coverage curves, since yield at all photon energies is increased by lowering the barrier.

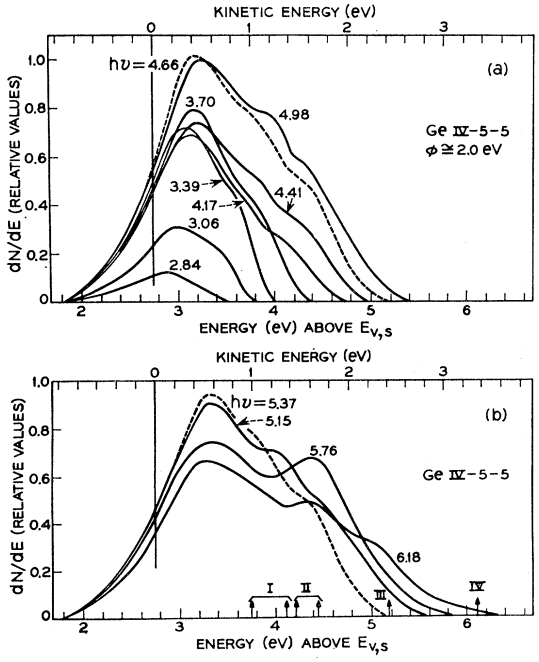

FIG. 17. Energy distributions from cesium-covered germanium at various photon energies.

The energy distributions for different photon energies at the same cesium coverage for a cleaved 0.3 Ω cm p-type germanium sample are shown in Fig. 17(a) and (b). A coverage a little short of a full monolayer with a work function of 2.0 eV has been chosen here since the structural features are obscured at full coverage (work function of ~1.6 eV), by the very large yield of low-energy electrons just above the escape envelope. Peaks I, II, and III seen in Fig. 16 are evident here, while peak IV is only seen at 6.18 eV on an expanded vertical scale. Note that peaks I and II move by several tenths eV in energy position as $h\nu$ varies. The features are summarized in Table IV.

Band-Bending Effects for Germanium

Both yield and energy distributions have been measured and compared for Cs-covered n-type (~0.005 Ω cm) and p-type (~0.005 Ω cm) germanium samples. As was already found for the clean-cleaved case,[4] band-bending effects are far less pronounced than for silicon. The yield of the p-type sample does not differ significantly from that for the n-type for high photon energies, but begins to rise above it at photon energies below 3.0 eV. Between 3.0 eV and the threshold of ~1.6 eV for each, the p-type yield becomes about twice that of n-type. The energy distributions do not disclose a noticeable shift toward higher KE for the peaks in the p type compared to the n-type sample.

This insensitivity to bulk doping in samples where the potential profile is estimated to differ by one whole energy gap in a distance of ~100 Å beneath the surface is somewhat surprising. It suggests that the mean escape depth for emitted electrons is appreciably shorter for germanium than for silicon, and that only for photon energies below ~3 eV is this escape depth long enough to sample space-charge band bending even in highly doped samples.

Interpretation and Assignment of Structure for Germanium

Considering the yield, reflectivity and distribution data together, the following can be said. We will refer to

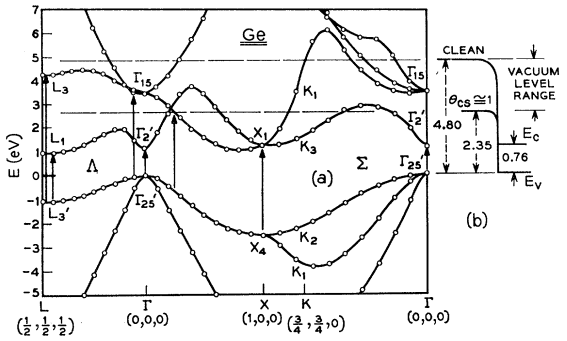

FIG. 18 (a). Energy-versus-**k** diagram for germanium by the pseudopotential calculations of Cohen and Phillips (Ref. 37), (b) Energy levels for the clean and cesium-covered (111) surface.

the E-versus-**k** diagram for Ge computed by Cohen,[37] Fig. 18. (See also suggested structural assignments of Cohen and Phillips for Ge in Ref. 37.)

(1). The rapid rise in yield at 2.9 to 3.2 eV has no clear cut corresponding structure in R or ϵ_2. The emitted electrons are seen from the distributions to appear just above the escape envelope at low KE, or at $E\cong 2.4$ to 3.0 eV. These low-energy electrons predominate over all others when the work function is lowered another 0.5 eV at full Cs coverage. Transitions near $\Gamma_{25'} \rightarrow \Gamma_{15}$ could explain both photon and KE features of these electrons. Primary electrons degraded from higher energies by both pair production and phonon losses, as well as secondaries arising from pair production undoubtedly add to the lowest energy group seen in the distributions.

(2). The sharp dip at 4.3 eV in yield corresponding to the peak in R and ϵ_2 near that energy has no feature in the distribution and thus is probably at least in part due to $X_4 \rightarrow X_1$ transition as for silicon. (This same feature persists in all the cesium-covered III–V compounds studied by photoemission.[37])

(3). The sharp rise in yield from 4.4 to 4.8 eV apparently results from added electrons with energies spread over the range $E=3.4$ to 4.4 eV, principally in peaks I and II.

(4). The peak in yield at 5.4 to 5.5 eV is associated with a sudden increase in peak II at $E=4.45$ eV. This seems to fit closely in both $h\nu$ and E to $L_{3'} \rightarrow L_3$ transitions.

(5). The reversal of the downward trend in yield at $\sim$5.8 eV corresponds to the appearance of peak III electrons in the distribution at $h\nu > 5.76$ with $E\cong 5.3$ eV. Transitions from the upper valence band to the second or fourth upper conduction bands which have critical points in the Σ region could account for this.

(6). Peak IV, appearing at $h\nu \geq 6.18$ eV and $E=6.10$ eV, may be due to the other of these same two critical points.

The behavior of peaks in the distributions near II and III may be more complicated than implied above, involving movement with $h\nu$ of three separate peaks instead of two. Definite assignment of structure in either yield or distributions for Ge must await the type of calculation Brust has performed for Si.

[37] M. L. Cohen and J. C. Phillips, Phys. Rev. (to be published).

ACKNOWLEDGMENTS

The authors are indebted to E. O. Kane for much advice and encouragement, and to both E. O. Kane and D. Brust for the prepublication access to results of their computations. We also thank J. C. Phillips, M. L. Cohen, and T. E. Fischer for helpful discussions and A. A. Studna, B. Hennion, and W. Emslie for patient and skillful technical assistance.

APPENDIX

Energy-Distribution Distortions

Ideally, total energy distributions should be taken using a small spherical emitter located inside a large concentric spherical collector, both electrodes having uniform surface potential. The nonideal situation can be analyzed as to the effect upon distributions due to (a) nonideal geometry, (b) nonuniform collector potential, and (c) nonuniform emitter potential and fringe fields near the emitter. The latter two can be lumped together because their effects upon distributions are the same.

The effect of nonideal geometry is to convert some of the electrons' initial energy into tangential kinetic energy relative to the collecting surface. Thus some electrons graze the collector but fail to be collected even though they have sufficient energy. This effect thus displaces energy distributions toward *lower* kinetic energy. In the simple spherical case, due to the finite emitter size, the magnitude of this error of the measured versus true energy at collection is greatest for tangentially emitted electrons and is given by

$$\delta E/E \leq (r_e/r_c)^2, \qquad \text{(A1)}$$

where r_e and r_c are the emitter and collector radii, respectively. Neglecting for the moment the fact that the fields in the present geometry are highly nonradial, and that the emitter is not at the center of the collector, we have $r_e \sim 0.5$ cm and $re \cong 2$ cm so that $(r_e/r_c)^2 \sim 0.06$, which is small. The effects of the nonradial fields are very difficult to estimate but they will be partially compensated by the fact that the corners on the present enclosure will trap many electrons that might return to the emitter in a sphere. An empiricial limit can be placed on the smearing of our distributions by this geometrical factor from the fact that in certain triangular shaped distributions we have obtained, the high-energy sides have risen from zero to their maximum value in a little over 0.15 eV. Hence we conclude that the geometrical factor smearing is less than this and thus small compared to most of the structure in our distributions. We also note that for this type of distor-

tion, the relative smearing $\delta E/E$ is equal in both high- and low-energy portions of the distributions (the displacement δE actually increases with E) but its value depends strongly on the *direction* of the emitted electron.

The effect of a nonuniformity ΔV in collector potential is to smear all portions of the energy distribution equally by the amount $f\Delta V$, where $f \leq 1$ and is determined by the patch structure on the collector. Again from the above-mentioned sharp, high-energy edge observed, we conclude that our gold-coated collector is uniform in potential to ~ 0.1 eV.

The effect of nonuniform emitter potential and fringe fields, on the other hand, is to smear out drastically the *low-energy end* of the distribution, making the saturation behvavior poor, but to leave the high-energy end of the distribution unaffected. This is simply seen by realizing that a low-energy electron, and particularly one that starts in a direction toward patch or fringe fields, will not be able to surmount even a small potential barrier near the emitter. It can thus not reach the collector until the collector field at the emitter exceeds the fringe field. This may require many volts on the collector since it is relatively far from the emitter. Electrons having high initial energies greater than the patch or fringe potential barriers, on the other hand, will pass over them and reach the collector, where they can then be correctly sorted as to energy.

It is clearly this type of distortion that has been the most serious in the present work and chiefly so for the partially covered surfaces. Here distributions for low photon energies (KE of emitted electrons of ≤ 2 eV) show spurious spreading of the low-energy sides of many tenths of an eV, and hence cannot usually yield reliable information. Fortunately, distributions even at low KE for the clean surfaces before Cs converge (no fringe or patch fields), or the high-energy portions of any other distribution, can still yield reliable information.

Four-Point-Probe Limitations

While surface and bulk conductance are in parallel in a four-point-probe measurement on a surface, use of 50 000 Ω cm (p type) bulk silicon permitted detection of changes in surface conductance as small as 0.05 μmhos per square in the cleaved samples. If the surface and bulk are of opposite conductivity-type, they are separated by an intrinsic region, and the potential drop measured between the two center probes depends upon whether or not the four probes make good contact to both surface and bulk. If so, conductances are still additive and results valid. If no contact is made to an n-type surface on a p-type bulk, the condition which prevails for Cs-coated Si and Ge, the potential drop across the center probes measures only the bulk conductance, so that an increase of n-type surface conductance as cesium is added would not be seen. It is possible that this was responsible for the erratic results and lack of strong n-type conductance found in this work. To check this, an n-type bulk should be used.

When the two conductances are additive, i.e., when good contact exists to both the surface layer and the bulk, we can separate the problem into an "infinitely" thin sheet of conductivity σ_s mhos per square carrying a current I_s plus a semi-infinite solid of conductivity σ_b $(\Omega\ \text{cm})^{-1}$ carrying a current of I_b. Then

$$\begin{aligned} I/V &= I/V(I_s+I_b) \\ &= k_s\sigma_s + k_b\sigma_b S, \end{aligned} \tag{A2}$$

where S is the probe spacing, (1 mm), $k_s=\pi/\ln 2$ and $k_b=2\pi$. When only the surface conductance changes, $\Delta(I/V)=k_s\Delta\sigma_s$. Note that for zero surface conductance, since $\sigma_b = 1/50\,000$ $(\Omega\ \text{cm})^{-1}$, we should have

$$\begin{aligned} V/I &= L/k_b\sigma_b S \\ &= 80\,000\ \Omega. \end{aligned} \tag{A3}$$

Since measured V/I values reached a maximum of $\sim 400\,000\ \Omega$ at what was presumably near zero surface conductance we must conclude that the narrow sample height (~ 1.5 mm) compared to the spacing between outer probes (3 mm) raised the apparent resistance by a factor of $\sim 5X$. Since the narrow sample reduces the surface conductance path more strongly than the bulk conductance path (the *depth* of the sample was large compared to outer probe spacing), we can assume the surface conductance changes were at least 5× larger than measured.

Evidence That the Surface is n-Type from Yield Curves

(1). All electrons in the "flat-band" sample originate from material where $E_F - E_V$ is nearly that at the surface.

(2). Nearly all electrons in n^{++} and p^{++} samples originate from material where $E_F - E_V$ is either $\sim E_G$ or ~ 0, respectively.

(3). Since the flat-band resembles the n^{++} sample, the flat-band surface values of $E_F - E_V$ is $\sim E_G$, so the surface is strongly n type.

(4). Since the work function of all three surfaces is ~ 1.6 eV, and since χ for a monolayer of cesium should be independent of bulk doping, the value of $E_F - E_V$ at the surface must be the same for all samples, and hence, all three must be strongly n type.